Silver Chloride Clusters and Surface States

ARTICLE *in* THE JOURNAL OF PHYSICAL CHEMISTRY B · JUNE 1999

Impact Factor: 3.3 · DOI: 10.1021/jp990701m

2 AUTHORS, INCLUDING:

Gion Calzaferri
Universität Bern
290 PUBLICATIONS **6,716** CITATIONS

Silver Chloride Clusters and Surface States

Stephan Glaus and Gion Calzaferri*

Department of Chemistry and Biochemistry, University of Bern, Freiestrasse 3, CH-3012 Bern, Switzerland

Received: February 26, 1999; In Final Form: May 7, 1999

Single-crystal or very compact AgCl materials are hardly light sensitive. In presence of adsorbed Ag^+ ions, AgCl precipitates with their correspondingly large surface area, however, lead to the discovery of photography on paper by Henry Fox Talbot in 1834 and were recently found to act as a catalyst for sustained photocatalytic oxidation of water to O_2. How large must a cluster be so that the inner atoms can be regarded as bulk? How do the surface atoms differ from inner ones? What is the difference between atoms at the corner, the edge, and the plane? What happens upon adsorbing water molecules and solvated Ag^+ ions on the AgCl cluster surface? Of what type are the first electronic transitions of such clusters, how large is their oscillator strength, and how are they influenced by adsorbed silver cations? Cubic $(AgCl)_n$ clusters with $n = 4$, 32, 108, and 256 have been studied by means of MO calculations and compared with the AgCl molecule and with the infinite AgCl crystal. The Ag−Cl distance was found to increase by 0.35 Å from AgCl to $(AgCl)_4$ and by 0.13 Å to $(AgCl)_{32}$, but then the changes become small, 0.02 Å from $(AgCl)_{108}$ to $(AgCl)_{256}$, despite the fact that the latter still contains 58% surface atoms. The HOMO is made up of Cl lone pairs. It changes little from AgCl to $(AgCl)_4$, then increases smoothly until no significant change is observed after $(AgCl)_{108}$. The lowest unoccupied orbitals are of the 5s(Ag) type and can be identified as *sur*face *s*tate levels (SURS) mainly localized at the corners. The next higher levels extend over the whole cluster. They correlate with the lower edge of the conduction band of the crystal. The charges of the innermost $(AgCl)_{108}$ species are almost the same as those of the innermost $(AgCl)_{256}$. These results lead to the conclusion that the $(AgCl)_{108}$ is sufficiently large for studying the influence of adsorption of an H_2O and of $Ag^+(H_2O)_2$. The largest stabilization of H_2O on $(AgCl)_{108}$ is observed when it is coordinated to Ag^+ at a corner site, which is slightly favored with respect to an Ag^+ site at the plane. Water coordinated to Ag^+ in the plane and on the edge has only minor influence on the SURS and no influence on the HOMO region. However, coordination at the corner shifts the SURS by about 0.5 eV to higher energy. Although the $[Ag(H_2O)_n]^+$ ($n = 2$, 4, 6) species have been investigated, the most direct way to study the interaction of solvated silver ions with an $(AgCl)_n$ cluster is to choose $[Ag(H_2O)_2]^+$. We distinguish between a silver site, a chloride site, an interstitial site, and points in between. The position with the Ag^+ of the aquocomplex directly on top of an Ag^+ of the cluster was found to be the most stable. The frontier orbital region of the $(AgCl)_{108}$ is little affected by the adsorbed aquocomplex. However, the 5s(Ag) level shows a bonding interaction with the surface at the most stable position. It is stabilized by interacting with 5p(Ag) which derives from the cluster LUMO region and lies more than 1 eV below the SURS of $(AgCl)_{108}$, thus forming a new low-lying surface state. Investigating the frontier orbital electronic dipole-allowed transitions, we found that for $(AgCl)_{108}$ the HOMO-to-SURS transition is very weak and that transitions to the next higher levels are forbidden. In the case of $[Ag(OH_2)_2]^+$ adsorbed on $(AgCl)_{108}$ electronic dipole allowed transitions, corresponding to a charge transfer from the 3p(Cl)-type HOMO of the cluster to the 5s(Ag) level of the aquocomplex, were found to be responsible for the increased photochemical activity observed for such systems.

1. Introduction

Silver chloride has been investigated intensively since the invention of photography on paper by Henry Fox Talbot around 1834. His light sensitive papers were made by first soaking in sodium chloride and then brushing with an excess of silver nitrate solution. The key to success was the observation that the paper was more sensitive to light if there was a deficiency of NaCl.[1,2] Other essential observations made by Talbot were that the picture could be stabilized by washing it with a large excess of NaCl and that the photographic paper could be sensitized by moderate daylight illumination. We have made similar observations about 160 years later when studying the ability of Ag^+-containing systems to photooxidize water to oxygen under conditions of a Cl^- deficiency.[3−6] There are now good reasons to assume that the first photographic papers of Talbot were based on the ability of silver chloride to oxidize water to O_2 in the presence of an excess of Ag^+. Recently we reported sustained photocatalytic oxidation of water to O_2 on AgCl layers on SnO_2:F-coated glass plates modified with a very thin gold layer.[6] The AgCl layer acts as a photocatalyst in the presence of a small excess of Ag^+ ions with a maximum O_2 evolution rate in the pH range of 4−6. The light sensitivity in the visible range is due to self-sensitization caused by reduced silver species. A system that has never been exposed to light is insensitive to the visible part of the spectrum; once irradiated in the near-UV, it becomes sensitive and is capable of

* Corresponding author: Telephone: +41 31 631 4226. E-mail: calza@solar.iac.unibe.ch.

10.1021/jp990701m CCC: $18.00
Published on Web 06/19/1999

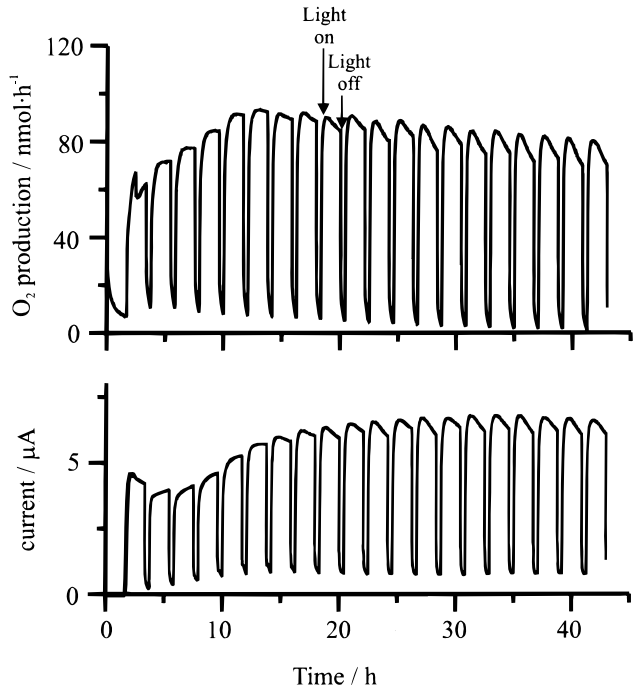

Figure 1. Photoelectrochemical experiment illustrating the photocatalytic oxidation of water on an electrochemically prepared AgCl-coated SnO_2:F electrode (1 cm^2) modified with a thin gold layer (100 Å) polarized at 0.0 V vs Hg/Hg_2SO_4. Oxygen production vs time (upper graph) and current vs time (lower graph).[6]

photooxidizing water in the whole visible range with a lower limit at 600−700 nm.[3−6] The photocatalytic water oxidation can be expressed as follows:

$$[n\mathrm{Ag}^+,m\mathrm{AgCl}] + \frac{r}{2}\mathrm{H_2O} \xrightarrow{\text{light}} [(n-r)\mathrm{Ag}^+,m\mathrm{AgCl},r\mathrm{Ag}^0] + r\mathrm{H}^+ + \frac{r}{4}\mathrm{O_2} \quad (1)$$

$$[(n-r)\mathrm{Ag}^+,m\mathrm{AgCl},r\mathrm{Ag}^0] \xrightarrow{\text{electrode}} [n\mathrm{Ag}^+,m\mathrm{AgCl}] + re^- \quad (2)$$

We show in Figure 1 an experimental result obtained in a flow system where the produced oxygen was continuously removed by a nitrogen stream, as an example. The light intensity at the AgCl-coated electrode was approximately 50 mW/cm^2 (Xenon arc lamp through a cold light filter) from which only part was absorbed. The turnover number for O_2 evolution with respect to the total amount of AgCl after 44 h when the experiment was stopped was 11, and it is obvious that much larger turnover numbers can be achieved. The photo current (eq 2) in these experiments is of reverse sign with respect to what has been known as Becquerel-type photo current.[7] It is well-known that single-crystal or very compact AgCl materials are hardly light sensitive. Pronounced light sensitivity is observed, however, for AgCl materials with a large surface. Such materials can, for example, be prepared by precipitation or by electrochemical techniques.[6]

While the electronic structure of AgCl crystals has been investigated in detail and can be considered as being well understood,[8−13] little is known about the electronic structure of AgCl layers, clusters, and surfaces. A theoretical study of AgCl clusters of relevant size is still missing. A reason for this is the fast-growing number of atoms in such clusters as illustrated in Scheme 1 for cubic $(AgCl)_n$ clusters. Nevertheless, calculating such systems and especially trying to extract relevant information from the resulting vast amount of numbers is challenging.

SCHEME 1: $(AgCl)_n$ Clusters; Grey Circles Represent the Silver Ions, White Circles the Chloride Ions.

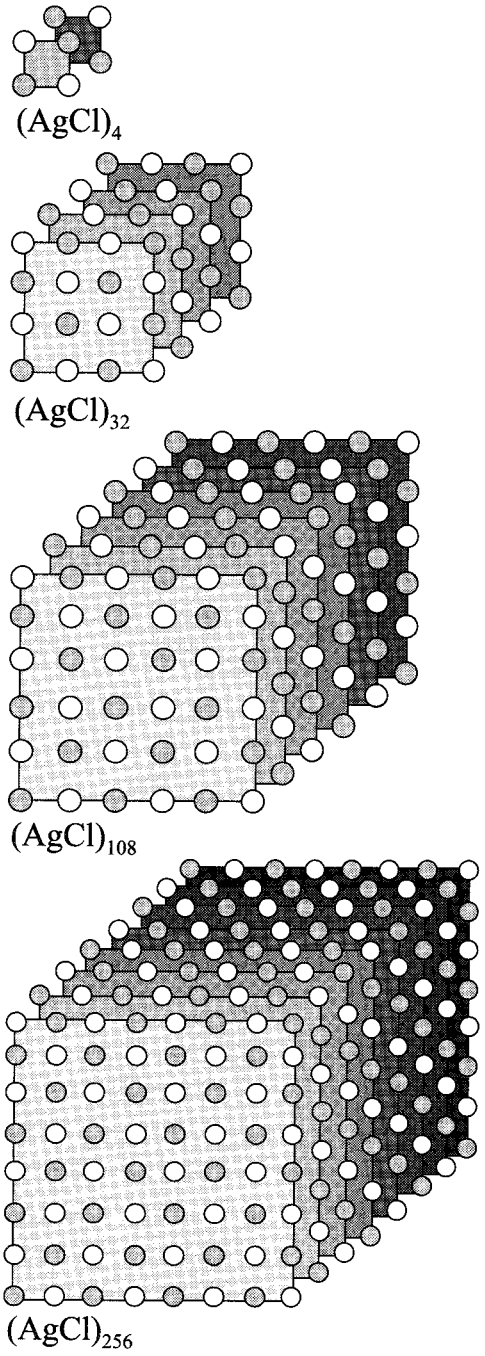

Questions relevant for improving our understanding of the chemical and photochemical properties of silver chloride nano and micro crystals are: How large must a cluster be so that the inner atoms can be regarded as bulk atoms? How do the surface atoms differ from inner atoms? What is the difference between atoms on the corner, the edge, and the plane? What happens if a water molecule or a solvated Ag^+ ion is adsorbed on the AgCl cluster surface? Of what type are the first electronic transitions of such clusters, how large is their oscillator strength, and how are they influenced by adsorbed silver cations? To find answers to these questions we have carried out molecular orbital calculation of EHMO-ASED type on the cubic clusters shown in Scheme 1. The surface states were analyzed by comparison with an extended AgCl crystal. It turned out that $(AgCl)_{108}$ was sufficiently large for studying adsorption of a H_2O molecule

TABLE 1: Slater Exponents Used for EHMO Calculations

element	AO	ζ_1	ζ_2	c_1	c_2
Cl	3s	2.18			
	3p	1.73			
Ag^+	5s	1.85			
	5p	1.30			
	4d	3.91	1.54	0.824	0.329
Ag^0	5s	1.70			
	5p	1.30			
	4d	3.91	1.54	0.824	0.329
O	2s	2.58			
	2p	2.27			
H	1s	1.30			

and of a $Ag^+(H_2O)_2$ complex. The results presented provide an understanding for the observations that nano AgCl clusters with their comparatively large surface area behave so differently with respect to very compact or single-crystal AgCl materials.

2. Computational Procedure.

MO and Oscillator Strength Calculations. Extended Hückel molecular orbital (EHMO) calculations[14] in their ASED (atomic superposition and electron delocalization) form[15,16] were performed using the ICON-EDiT[17] program package. The off-diagonal elements were calculated as[18]

$$H_{ij} = \frac{1}{2}KS_{ij}(H_{ii} + H_{jj}) \tag{3}$$

by using the distance−dependent weighted Wolfsberg−Helmholz formula[19]

$$K = 1 + k\left(\frac{\exp(-\delta(R - d_0))}{1 + (\delta(R - d_0 - |R - d_0|))^2}\right) \tag{4}$$

with $\kappa = 0.8$,[20] $\delta = 0.35$ Å^{-1}, and

$$k = \kappa + \Delta^2 - \Delta^4\kappa \quad \Delta = \frac{H_{ii} - H_{jj}}{H_{ii} + H_{jj}} \tag{5}$$

Equations 3−5 are implemented in ICON-EDiT[17] as default. H_{ii} and H_{jj} are the Coulomb parameters of the *i*th and *j*th atomic orbital. They have been determined by charge iteration; for details see refs 17, 21, 22. R is the distance between the atoms on which the atomic orbitals are located, and d_0 the sum of the *i*th and *j*th atomic orbital radii as calculated from the corresponding Slater exponents (cf. eqs 13 and 14 in ref 15). A two-body term was used to correct for the core−core repulsion.[15,17] The calculations were carried out with the Slater parameters listed in Table 1. We have reconsidered the charge iteration parameters for silver according to the procedure described in refs 21 and 22, and using the spectroscopic data for the Ag atom reported by Moore.[23] The corrected values are listed in Table 2 and implemented in ICON-EDiT[17] and BICON-CEDiT[24] as default.

The EHMO-ASED bond angle of the water molecule initially reported was much too large.[25] The reason was an overestimation of the antibonding 1s(H)−1s(H) interaction by the Wolfsberg−Helmholz formula. This problem can be overcome by choosing a smaller κ for the H−H interaction than for the O−H bond. The result of a calculation with $\kappa = 1.0$ and $\kappa = 0.2$ for the O−H and for the H−H interaction, respectively, is illustrated in Figure 2, which shows that the potential obtained by this procedure is good. Since also the other properties of H_2O are well described by this choice, it has been used throughout all calculations. The oscillator strength calculations have been carried out as described in refs 17 and 26.

TABLE 2: Charge Iteration Parameters for Calculating the Coulomb Integrals Used in EHMO Calculations

	configuration	d_2 (eV)	d_1 (eV)	d_0 (eV)
silver				
s VOIE	$4d^{10}5s^1$	0.5500	8.3900	7.5800
	$4d^95s^2$	0.3700	8.8800	8.8000
	$4d^95s^15p^1$	0.3100	9.7100	10.2300
p VOIE	$4d^{10}p^1$	0.7700	6.4600	3.8300
	$4d^9p^2$	1.1800	6.8600	8.1200
	$4d^95s^15p^1$	1.1800	6.8600	4.7600
d VOIE	$4d^{11}$	−3.9000	25.6000	0.0000
	$4d^{10}5s^1$	0.4600	12.6600	12.7700
	$4d^{10}5p^1$	0.8100	11.6700	14.4900
chlorine[a]				
s VOIE	$3s^23p^5$	1.6986	15.7089	25.2682
p VOIE	$3s^23p^5$	1.6726	13.1796	13.6880
oxygen[a]				
s VOIE	$2s^22p^4$	3.4654	22.8877	32.3353
p VOIE	$2s^22p^4$	3.4642	18.5668	15.7957
hydrogen[a]				
s VOIE	$1s^1$	13.6185	27.1776	13.6012

[a] Ref 22.

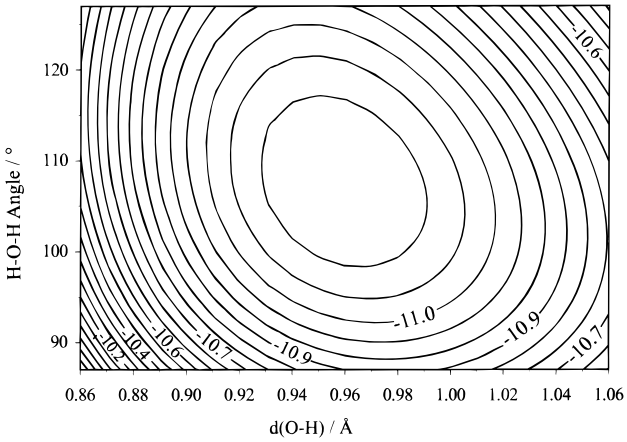

Figure 2. Calculated potential energy surface of H_2O. The minimum is at d(O−H) = 0.96 Å and α(H−O−H) = 107° with the π-type oxygen lone pair at −12.9 eV as HOMO.

Band Structure Calculations. Extended Hückel tight-binding[27] band structure calculations in their ASED form[25] were performed using BICON−CEDiT[24] with the same weighted Wolfsberg−Helmholz formula eqs 3−5 and the same parameters as for the ICON-EDiT calculations. The first Brillouin zone for the face-centered cubic AgCl lattice is given in Scheme 2. The Γ point at the center of the zone possesses the highest symmetry, while Λ, Δ, and Z denote lines of high symmetry. Density of states (DOS) and crystal orbital overlap population (COOP) calculations have been carried out with a set of 100 k-points[28] representing the face-centered cubic lattice.

3. Results and Discussion

The clusters investigated in this study are cubic AgCl units. By increasing the cluster size, as shown in Scheme 1, we finally end up with an infinite AgCl crystal. Other building blocks are the hydrated silver ions $Ag^+(H_2O)_n$, with $n = 2$, 4, 6. It is necessary to discuss them before approaching the $(AgCl)_n$ clusters.

The AgCl Molecule. The AgCl molecule has the tendency to form larger units in which the Ag^+ and the Cl^- are surrounded by six neighbors. The negatively charged complexes $AgCl_n^{(n-1)-}$ are also well-known. They are responsible for the solubility of silver chloride in concentrated aqueous Cl^- solutions.[29] It should be possible to prepare stable AgCl molecules in confined media

TABLE 3: Experimental and Calculated Data for the AgCl Molecule and the AgCl Crystal

	d(Ag−Cl)/Å				ΔE(HOMO−LUMO)/eV				D_e/eV				IP/eV	
	expt	this work	DFT-LDA[a]	SCF-HF	expt	this work	DFT-LDA[a]	SCF-HF	expt	this work	DFT-LDA[a]	SCF-HF	expt	this work
molecule	2.28[b]	2.34	[g]	2.44[c]	3.91[b]	4.4	[g]	[g]	3.22[b]	3.14	[g]	2.52[c]	11.0[d]	10.9
crystal	2.77	2.94[h]	2.73	2.96[e]	3.25	4.2[h] 3.2[i]	1.25	13.5[e]	5.40[f]	3.0[h] 3.1[i]	[g]	3.70[e]	[g]	10.3[h] 10.3[i]

[a] Ref 34. [b] Ref 31. [c] Ref 35. [d] Ref 32. [e] Ref 9. [f] Ref 36. [g] No data available. [h] ζ(3s(Cl)) = 2.18. [i] ζ(3s(Cl)) = 2.5 calculated for d(Ag−Cl) = 2.94 Å.

SCHEME 2. The First Brillouin Zone for the Face-Centered Cubic Lattice: Point Γ Is the Center of the Zone and Possesses the Highest Symmetry, L and X Are Points, and Λ, Δ, and Z Are Lines of High Symmetry.

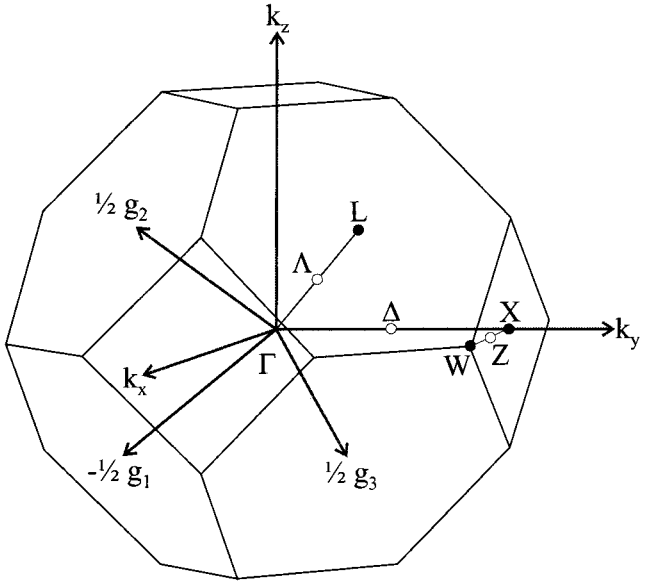

such as the cavities of zeolites, similar as has been shown recently for very small silver sulfide clusters.[30] However, only AgCl molecules in the gas phase have been reported so far. The dipole moment of AgCl is −5.70 D,[31] which is much smaller than the about −11 D one would expect for a purely ionic compound in a point mass approximation. We consider the correlation diagram shown in Figure 3. The HOMO and HOMO-1 levels are a doubly degenerate 3p(Cl) lone pair and a σ[5s(Ag)-3p$_z$(Cl)]-type orbital, respectively. The experimental first ionization energy has been reported to be 11 eV[32] and is well-reproduced by our calculation. It is instructive to compare it with those of a silver atom and of silver bulk which lie at 7.6 and 5.57 eV,[33] respectively, and with those of the Cl atom and the Cl_2, which are 13.1 and 11.48 eV, respectively. The LUMO is an antibonding σ*-orbital, mainly localized at the silver and therefore named σ*[5s(Ag)]. The HOMO−LUMO electronic transition occurs at 3.9 eV and is of 5s(Ag)←n[3p$_{x,y}$(Cl)] charge transfer (CT) type. Experimental data, data from our calculations, and calculations reported in the literature are summarized in Table 3.

The AgCl Crystal. To avoid complicated back folding, we have used a primitive unit cell spanned by three vectors starting in a cube corner pointing to the center of the adjoining vertexes to calculate the face-centered cubic AgCl crystal. The corresponding Brillouin zone is shown in Scheme 2. Electronic transitions in AgCl crystals are intensively discussed in the literature. The AgCl absorption spectrum shows a broad band starting below 400 nm.[37] An indirect band gap of 3.25 eV from the L to the Γ point has been observed in photoelectron spectra.[38] The direct band gap was found at Γ. Its energy was reported to be about 2 eV larger than that of the indirect L←Γ one. This interpretation is consistent with band structure calculations

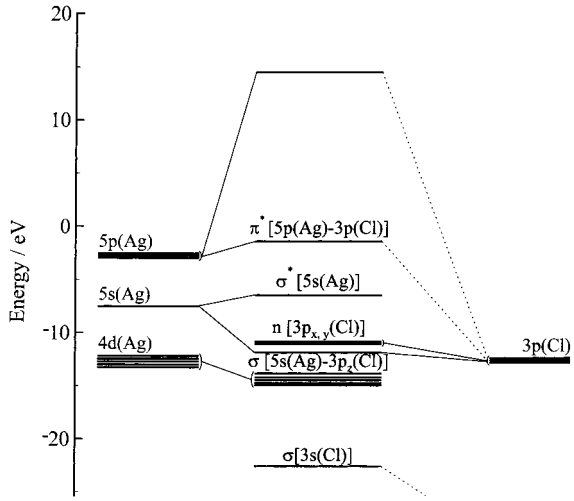

Figure 3. Correlation diagram of an AgCl molecule. On the left are the energy levels of the silver ion, and on the right are those of the chloride ion. The HOMO−LUMO electronic transition occurs at 3.9 eV and is of 5s(Ag)←n[3p$_{x,y}$(Cl)] charge-transfer type.

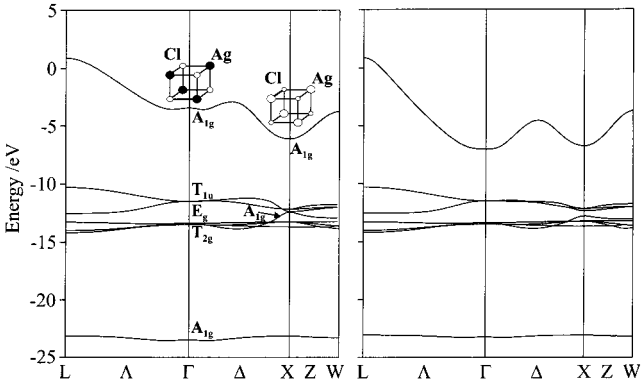

Figure 4. Band structure of an AgCl crystal along the symmetry lines Λ, Δ, and Z. The band structure on the left side has been calculated with ζ(3s(Cl)) = 2.18 and on the right with ζ(3s(Cl)) = 2.5.

reported by Aprà et al.,[9] Bassani et al.,[11] and Victora.[12] There is general agreement that the valence band consists of 3p(Cl)-type orbitals, while the conduction band is of 5s(Ag)-type. Results of EHTB-calculations are illustrated in Figures 4−6. We first discuss the band structures in Figure 4. Three main regions can be distinguished within the energy window shown. The flat band at about −23 eV derives from 3s(Cl) states. 3p-(Cl) and 4d(Ag) lie between −14 and −10 eV and mix slightly, the HOMO is of 3p(Cl)-type. The results obtained with the 3s-(Cl) Slater parameter reported in Table 2 are on the left side of Figure 4. They show the expected level ordering of the valence- and conduction band. However, the relative positions of the LUMO at the Γ and the X point are reversed, with respect to what is known from experiments. The reason for this can be understood by analyzing the orbitals at the respective high symmetry points. We found that the antibonding s-orbitals at Γ and the bonding s-orbitals at X shown in Figure 4 (left)

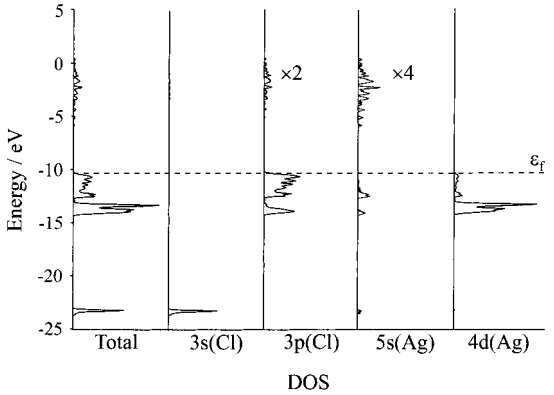

Figure 5. Density of states (DOS) and the contributions of 3s(Cl), 3p(Cl), 5s(Ag), and 4d(Ag) in the energy region from −25 to 5 eV. The dashed horizontal line indicates the Fermi level ϵ_f at −10.3 eV.

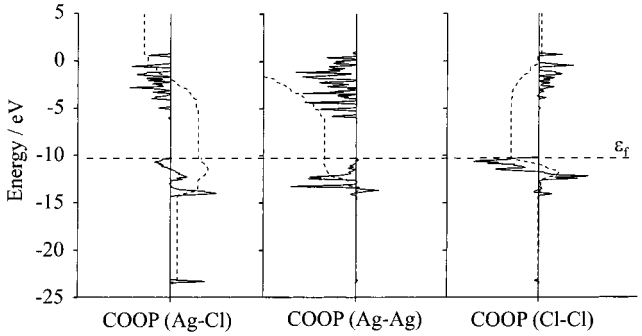

Figure 6. Crystal orbital overlap population (COOP) for all nearest neighbor interactions in an AgCl crystal. The solid lines give the COOP, and the dashed vertical lines represent the integrated values. The dashed horizontal line indicates the Fermi level ϵ_f.

determine the relative positions of this band. The interaction of the conduction band at X with the A_{1g} level in the valence band seems to be less important. From this one can expect that contraction of the 3s(Cl) orbital will significantly weaken the antibonding interactions at Γ. The result is that the conduction band comes down and that the indirect L←Γ band gap decreases in energy. At X we expect the reverse effect to occur, namely some destabilization of the conduction band. The result of calculations with $\zeta(3s(Cl)) = 2.5$ reported on the right side of Figure 4 shows that the effect is even more pronounced than expected. The LUMO starts at the same energy at L but comes down much faster than for the non contracted 3s(Cl) orbital. It reaches its minimum at Γ and then goes up as before and comes down at X again but not as deep as at the Γ point. The indirect L←Γ band gap is now found at 3.2 eV while the direct one is located at the Γ point at 4.4 eV, in agreement with the experiment. At point X we observe that the interaction of the LUMO with the A_{1g} level in the HOMO region is weakened. We conclude that contracted 3s(Cl) orbitals are needed for a correct description of the relative energy of the direct and the indirect band gap but that this contraction is of little consequence for the description of the valence band region. EHTB calculations on AgBr that have recently been reported[39] show qualitatively the same valence band features as we have described for AgCl. The conduction band of the AgBr crystal is, however, significantly different. At point X it decreases to low energy that leads to an indirect L←X band gap.

We turn to direct space by looking at the density of states (DOS) and the crystal orbital overlap population (COOP) of the infinite AgCl system in Figures 5 and 6. The DOS and the orbital contributions of 3s(Cl), 3p(Cl), 5s(Ag), and 4d(Ag) orbitals and the COOP are shown for the same energy window as used in Figure 4. The dashed horizontal line represents the Fermi level ϵ_f at −10.3 eV. The lowest region at −23 eV is dominated by 3s(Cl) orbitals. The next region is characterized by the typical sharp features caused by the T_{2g} 4d(Ag) orbitals with the 5s(Ag) and 3p(Cl) contributions. The valence band region is dominated by 3p(Cl) orbitals with some 5s(Ag) at the lower end and some 4d(Ag) contributions. The conduction band consists of almost pure 5s(Ag) orbitals. The first direct and indirect electronic transition are of 3p(Cl) to 5s(Ag) charge-transfer type. It is interesting that these LUMO←HOMO transitions are of the same kind as already encountered in the AgCl molecule. The integrated COOP in Figure 6 is represented by the vertical dashed line. The bonding Ag−Cl interaction is only slightly weakened by an antibonding region just below the valence band edge. However, the Ag−Ag and the Cl−Cl interactions are antibonding. Their integrated COOPs are both negative at the Fermi level. This is the reason for the larger Ag−Cl distance in the crystal compared to the molecule and the small clusters.

TABLE 4: Bond length $d(Ag^+-O)$ of $[Ag(H_2O)_n]^+$ (n = 2,4,6) Complexes[a]

coordination number	geometry	bond length $d(Ag^+-O)$/Å calcd	bond length $d(Ag^+-O)$/Å expt	$\Delta E_{stabilization}$ per H_2O/eV
2	linear	2.20	2.15	−0.60
4	tetrahedral	2.40	2.40	−0.81
6	octahedral	2.50	2.50	−0.58

[a] $\Delta E_{stabilization}$ is the calculated energy difference between the complex and the free Ag^+ and H_2O.

The $[Ag(OH_2)_n]^+$ Complexes. The coordination of the silver cation in water has been investigated by different methods.[40−43] There is general agreement that in the most stable solvated aquocomplex, the Ag^+ is tetrahedrally coordinated by four water molecules.[41] However, two-, four-, and six-coordinated complexes are known from crystallographic data, with linear, tetrahedral, and octahedral geometry, and mean Ag−O distances of 213, 240, and 250 pm, respectively.[44] Measurements of the thermodynamic data for the gas-phase reaction 6 have been reported.[40−43]

$$[Ag(H_2O)_2]^+(g) \rightarrow Ag^+(g) + 2H_2O(g) \qquad (6)$$

The values found for the free energy $\Delta G°$, the entropy $\Delta S°$, and the enthalpy $\Delta H°$ are 184 kJ/mol, 188 J/(mol K) and 236 kJ/mol, respectively. The electronic spectra of silver aquocomplexes which are colorless have been studied by Texter et al.[45] They reported broad bands with maxima at 225, 210, and 192 nm. The 225 nm band coincides with the long wavelength absorption band of silver aquocomplexes in zeolite A cavities.[46] We studied the geometry and the electronic structure of the three $[Ag(OH_2)_n]^+$ aquocomplexes with n = 2, 4, and 6. A linear, a tetrahedral, and an octahedral complex were found to be stable for n = 2, 4, and 6, respectively, with increasing Ag−O bond length, in good agreement with experimental data.[44] Planar $[Ag(OH_2)_4]^+$ was found to be unstable while the tetrahedral complex is the most stable species. The preference of tetrahedral with respect to octahedral coordination corresponds to what is generally expected for a d^{10} central atom from angular overlap reasoning.[47] This is also true for the T_d symmetry of the $[Ag(OH_2)_4]^+$ with respect to a planar arrangement, because OH_2 is a weakly interacting ligand. The stabilization energy $\Delta E_{stabilization}$ reported in the last column of Table 4 is the calculated energy difference between the complex and the separated Ag^+ and H_2O. In Figure 7 we show a correlation diagram connecting different

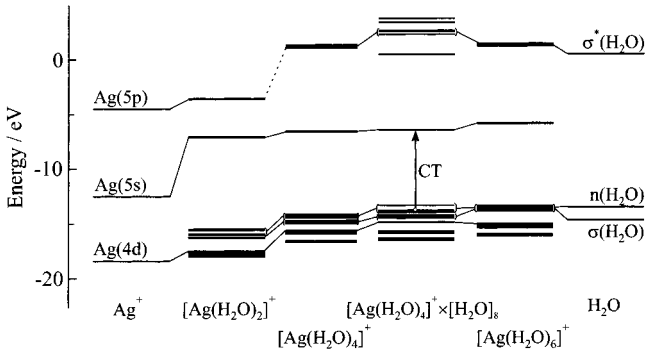

Figure 7. Correlation diagram of silver aquocomplexes. On the left energy levels are of Ag^+, on the right the energy levels of H_2O are shown. The arrow indicates an electronic charge-transfer transition CT from the inner shell water lone pairs to the 5s(Ag) orbital.

silver aquocomplexes. It is essential for the understanding of their electronic structure.

In all cases the LUMO is well separated from all other levels. It shifts little in energy and consists mainly of 5s(Ag) orbitals. We therefore name it the 5s(Ag) level. The character of the HOMO is always of $n(H_2O)$-type. The positive charge of the central atom stabilizes this level. This stabilization is more pronounced for small coordination numbers. The larger the coordination number, the better the charge can be distributed. We focus on the most stable complex $[Ag(OH_2)_4]^+$. In water it is surrounded by a next shell of water molecules which helps to dilute the positive charge of the central atom. This has been simulated by adding 8 outer shell water molecules. They have been arranged so that each oxygen of the outer shell water is bridged to an inner shell hydrogen atom. The HOMO obtained in this case is a water lone pair which belongs to the outer shell water molecules. More interesting is the HOMO-1 level. Its character is approximately 95% of inner shell $n(H_2O)$ type. The first electronic transition of solvated silver ions can therefore be described as 5s(Ag)←$n(H_2O)$ charge transfer, as indicated in Figure 7. The computed oscillator strength for this transition is 0.03, in reasonable agreement with the oscillator strength of the 225 nm band measured in a 1.4×10^{-4} M $AgClO_4$ aqueous solution which we found to be 0.01.

The $(AgCl)_n$ Clusters. We model $(AgCl)_n$ clusters as shown in Scheme 1. The smallest one consists of 8 atoms which are all on the surface. What are the most relevant changes which occur with increasing cluster size and at what size do the innermost cluster properties become almost identical to those of the extended crystal? To find an answer we have evaluated the development of the AgCl distance, of the frontier orbitals, and of the charge distribution.

The optimized AgCl distances, reported in Figure 8, show an increase of 0.35 Å from AgCl to $(AgCl)_4$ and of 0.13 Å to $(AgCl)_{32}$, but then the curve flattens and changes become small, only 0.02 Å from $(AgCl)_{108}$ to $(AgCl)_{256}$. The sharp increase of the AgCl distance at the beginning and its smooth continuation is due to the antibonding Ag−Ag and Cl−Cl interactions reported in Figure 6. When comparing the $(AgCl)_{256}$ with the infinite crystal we should keep in mind that the former still consists of 58% surface atoms. This becomes evident when inspecting the position of the frontier orbitals in Figure 9. The energy of the HOMO changes little between AgCl and $(AgCl)_4$ because it consists of Cl lone pairs in both cases. Then it increases smoothly but no significant change is observed after the $(AgCl)_{108}$. The lowest unoccupied orbitals of the clusters show a completely different behavior. They are of 5s(Ag)-type already in the AgCl as seen in Figure 3. In the larger clusters

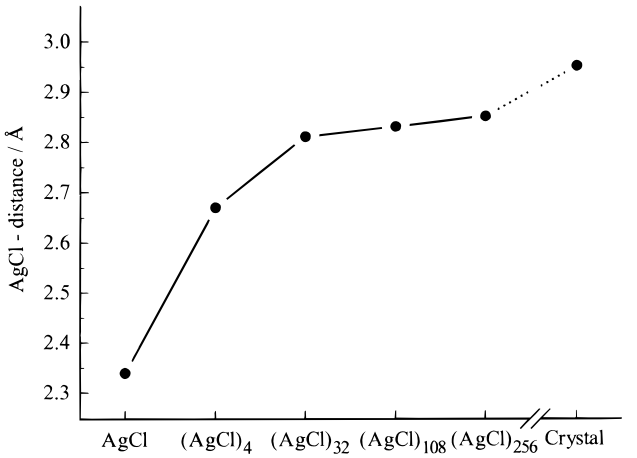

Figure 8. Calculated AgCl distance as a function of the cluster size. The line between $(AgCl)_{256}$ and the crystal is dashed, because of the cluster surface states.

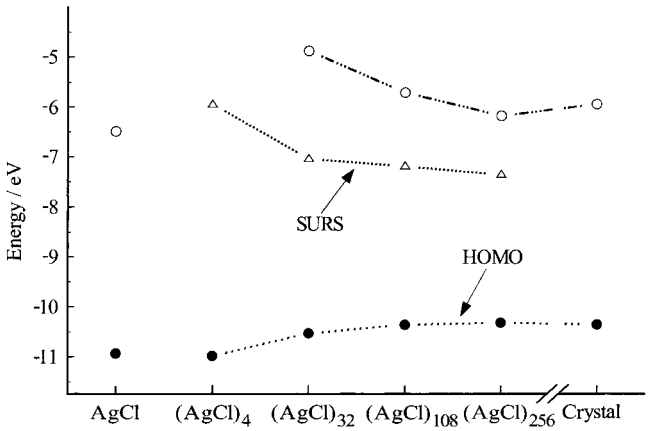

Figure 9. Frontier orbitals in dependence of the $(AgCl)_n$ cluster size.

they are mainly localized at the corner atoms and can therefore be identified as surface state (SURS) levels[48,49] which obviously do not exist in the infinite extended crystal. The next higher level expands over the whole cluster. It correlates with the lower edge of the conduction band. The energy level diagram of the $(AgCl)_{108}$ shown in Figure 10 gives more details. At −7 eV we find 4 levels of 5s(Ag) type which are localized at the 4 corner Ag atoms and can therefore be described as typical SURS. The next higher levels at −5.9 eV and above show a mixing of bulk and surface atoms. They keep their character in the infinite crystal. The HOMO region consists of mainly 3p(Cl)-type orbitals which expand over the whole cluster and correlate with the edge of the valence band of the crystal.

So far we have distinguished only between surface and bulk atoms. A more detailed picture in which single atoms can be separately discussed is provided by the charge calculated from Mulliken population analysis. In Figure 11 we distinguish between the charges of chloride ions, shown on the left, and the charges of the silver ions, shown on the right. Large and dark balls represent large positive charges in the case of silver and large negative charges in the case of chloride. The $(AgCl)_{108}$ cluster is shown at the top. The chloride ions at the corners and also at the edges are significantly more negative than the others. It is remarkable that their charges remain already constant after the outermost shell. This is different for the silver. Again the corner and the edge atoms bear the largest charges. But there are significant changes among the others. It is obvious that a single shell is not sufficient to keep their charges constant. We therefore also show the results obtained for the $(AgCl)_{256}$. The

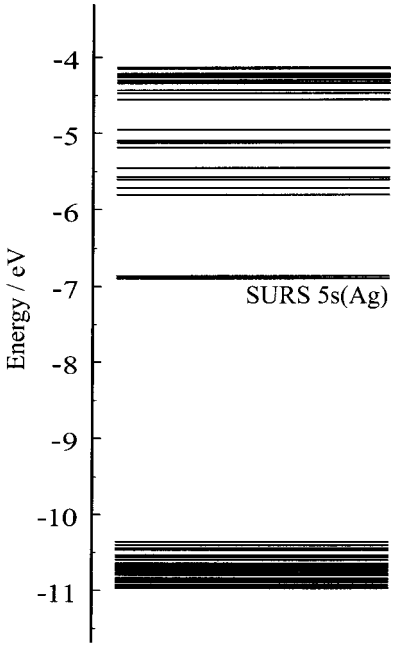

Figure 10. Energy levels of an $(AgCl)_{108}$ cluster. The surface states (SURS) reduce the HOMO−LUMO gap by about 1 eV. The SURS consist of 5s(Ag) orbitals, located at the corner of the cluster.

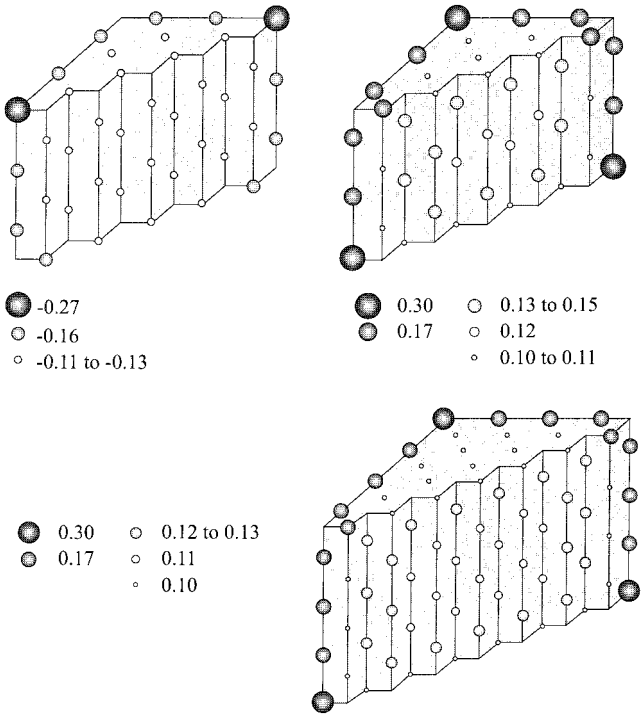

Figure 11. Mulliken charge distribution of $(AgCl)_{108}$ and $(AgCl)_{256}$. The drawing is made so that the corner, the edge, the plane, and the core atoms can be recognized. Left: charge distribution of the chloride ions in $(AgCl)_{108}$. Right: charge distribution of the silver ions in $(AgCl)_{108}$ and $(AgCl)_{256}$.

main observation is that all charges of the innermost $(AgCl)_{108}$ atoms are nearly the same as those of the innermost $(AgCl)_{256}$ atoms. The change of the AgCl distance (Figure 8), the behavior of the frontier orbitals (Figure 9), and the charge distribution lead to the conclusion that the $(AgCl)_{108}$ is sufficiently large to model important features of $(AgCl)_n$ nano clusters. For this reason, adsorption of a water molecule and of $Ag^+(H_2O)_2$ species have been studied on $(AgCl)_{108}$.

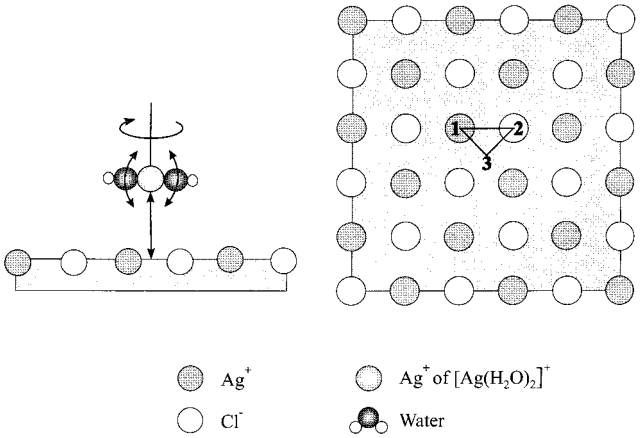

Figure 12. Investigated positions of the $Ag^+(OH_2)_2$ on the $(AgCl)_{108}$ cluster surface. The distance to the surface, the angle about the indicated axis, and the $O-Ag^+-O$ angle have been varied.

TABLE 5: Calculated *d*(Ag−O) Distances and Stabilization Energies of H_2O on the $(AgCl)_{108}$ Surface

	d(Ag−O)/Å	$\Delta E_{stabilization}$/eV
plane	2.9	−0.20
edge	2.9	−0.17
corner	2.7	−0.29

Water on an $(AgCl)_{108}$ Surface. The interaction of a H_2O molecule on an $(AgCl)_{108}$ surface is evaluated. We distinguish between a silver site (position 1), a chloride site (position 2), an interstitial site (position 3), and points between, as indicated on the right of Figure 12. The calculations have been carried out by assuming that the oxygen points toward the surface and that the C_2 axis of H_2O is normal to it. Rotation around the C_2 axis has only minor influence on the stabilization energy. We therefore decided not to consider this any further. In the middle of an $(AgCl)_{108}$ cluster plane the most stable situation corresponds to a water molecule opposite to an Ag^+, similar as in the silver aquocomplexes, with an equilibrium distance of 2.9 Å and a stabilization energy of 0.2 eV with respect to the separated H_2O and $(AgCl)_{108}$. On moving along the connecting line from position 1 to position 2, the energy remains nearly constant until we approach the Cl^- where it rises significantly. The same is true when traveling from positions 1 to 3 to 2. The situation is similar for a water molecule placed on the edge, however, the stabilization energy is slightly smaller. The largest stabilization is observed when H_2O is coordinated to Ag^+ at a corner site, which is favored by about 0.1 eV with an equilibrium distance of 2.7 Å, see Table 5. It is interesting to observe that the H_2O coordinated to Ag^+ in the plane and on the edge have only a minor influence on the SURS levels, illustrated in Figure 10, and no influence on the HOMO region. However, those coordinated to the corner shift the SURS of the corresponding Ag^+ level by about 0.5 eV to higher energy. When the four corner Ag^+ are coordinated by H_2O, all SURS shift by this amount of energy.

$Ag^+(H_2O)_2$ on an $(AgCl)_{108}$ Surface. The easiest way to study the interaction of solvated silver ions with a $(AgCl)_n$ cluster is to choose $[Ag(H_2O)_2]^+$. We distinguish between a silver site (position 1), a chloride site (position 2), an interstitial site (position 3), and points between, similar to what has been done for the H_2O. We allow rotation of the complex about the axis normal to the surface, variation of the distance to the

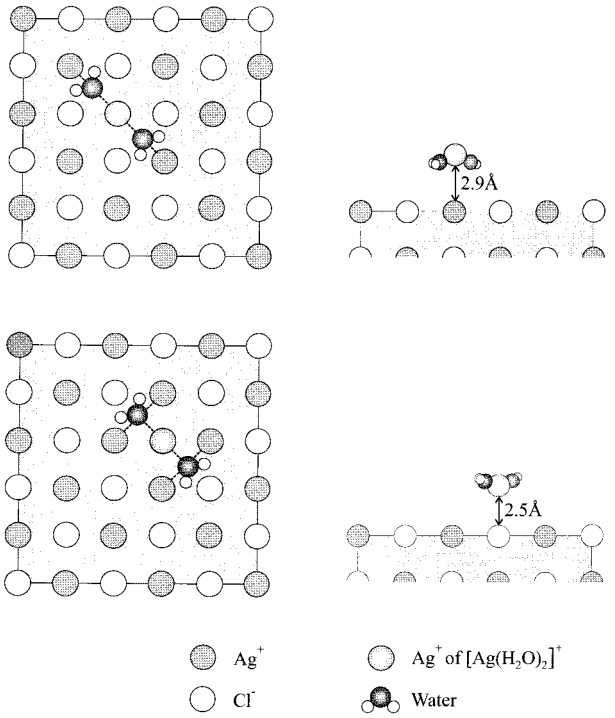

Figure 13. The two stable positions 1 (upper part) and 2 (lower part) of $[Ag(OH_2)_2]^+$ on the $(AgCl)_{108}$ surface. The $O-Ag^+-O$ angle is 160° and 200°, respectively. On the left, bonding interactions are dashed.

surface, and variation of the $H_2O-Ag^+-OH_2$ angle as indicated in Figure 12.

Position 1, where the Ag^+ of the aquocomplex is directly above an Ag^+ of the cluster, is the most stable. In this configuration the two H_2O are bent by about 10° toward the surface, as illustrated in Figure 13. At position 2 the Ag^+ is directly above a Cl^-. It corresponds to a local minimum, with two H_2O bent by about 10° away from the surface, which is slightly less stable than position 1. At position 1 the two oxygen atoms of the ligands are stabilized by interacting with the neighboring silver ions, while at position 2 antibonding interaction with neighboring chloride ions becomes dominant. On the other hand the Ag^+ of the aquocomplex is more stabilized at position 2, which is expressed in the shorter Ag^+ surface distance. The former effect is, however, stronger and makes position 1 the most stable.

The frontier orbital region of the $(AgCl)_{108}$ cluster is little affected by the adsorbed aquocomplex with the exception of the 5s(Ag) level of the $[Ag(H_2O)_2]^+$, which shows a bonding or an antibonding interaction with the surface, depending on the position as illustrated in Figure 14. At position 1 the 5s energy level is stabilized by about 1 eV with respect to the aquocomplex and lies more than 1 eV below the SURS of $(AgCl)_{108}$, thus forming a new low-lying surface state. This single level rises quickly in energy, to the region of the levels above the SURS, when the $[Ag(H_2O)_2)^+]$ is shifted to position 2, because here the Ag^+ experiences an antibonding interaction with a 3p(Cl) orbital. The stabilization at position 1 is due to the opposite effect, namely a bonding interaction of the 5s(Ag) of the complex with 5p(Ag) deriving from the cluster LUMO region.

We now investigate the frontier orbital dipole-allowed electronic transitions of the $(AgCl)_{108}$ cluster and the influence caused by an adsorbed $[Ag(H_2O)_2]^+$. For $(AgCl)_{108}$, the HOMO-to-SURS transition is very weak ($<10^{-4}$) and those to the next higher levels are forbidden. We consider transitions to be

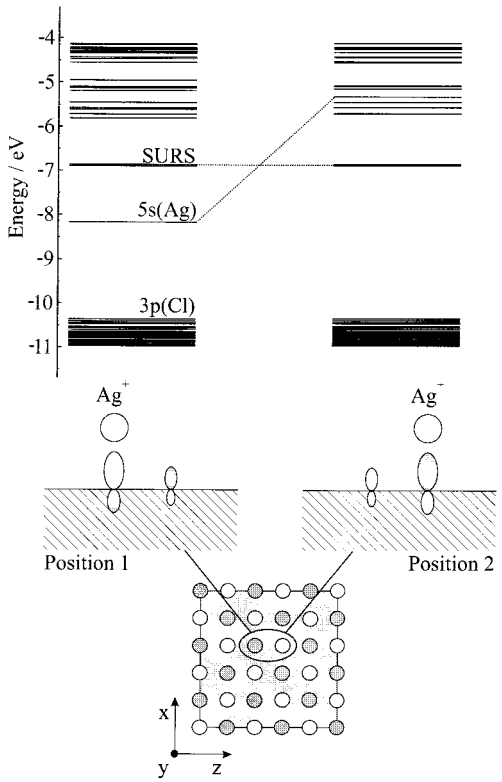

Figure 14. The 5s(Ag) levels deriving from $[Ag(OH_2)_2]^+$ on $(AgCl)_{108}$ positions 1 left) and 2 (right), qualitatively explained below.

TABLE 6: Calculated Oscillator Strength for the 5s(Ag)←HOMO Electronic Transition of the $(AgCl)_{108}-[Ag(H_2O)_2]^+$ System (the HOMO consists of three nearly degenerate levels)

E_i	E_f	ΔE/eV	$f_{ed,x}/10^{-3}$	$f_{ed,y}/10^{-3}$	$f_{ed,z}/10^{-3}$	$f_{ed,tot}/10^{-3}$
position 1						
HOMO	LUMO	2.2	0.51	3.07	0.51	4.09
position 2						
HOMO	LUMO+12	5.0	1.76	0.32	1.74	3.82

forbidden when the calculated oscillator strength is smaller than 10^{-5}. This means that these nano clusters are expected to be colorless, despite the low-lying SURS. This changes, however, in case of the $[Ag(OH_2)_2]^+-(AgCl)_{108}$ system because now weakly allowed transitions to the 5s(Ag) level of the aquocomplex can be observed. In case of the more important position 1, this transition corresponds to a charge transfer from the cluster 3p(Cl)-type HOMO to the Ag^+ of the aquocomplex with an oscillator strength of 0.004. At position 2 this transition changes mainly in energy but not in intensity and type, see Table 6.

Placing $[Ag(H_2O)_2]^+$ on all six faces of the $(AgCl)_{108}$ (position 1), the oscillator strength rises more than 6 times, namely to 0.032. This means that cooperation takes place. It is likely that these CT transitions are responsible for the well-known increased photochemical activity of nanocrystalline AgCl materials in the presence of an excess of silver ions.

4. Conclusions

Computational results obtained for AgCl, for an infinite AgCl crystal, for H_2O, and $[Ag(H_2O)_n]^+$ with $n = 2, 4, 6$ have been found to be in good agreement with experimental results. Based on this we have presented a study of $(AgCl)_n$ ($n = 4, 32, 108, 256$) clusters and we have investigated the influence of adsorbed H_2O and $Ag^+(H_2O)_2$ on the electronic structure of $(AgCl)_{108}$.

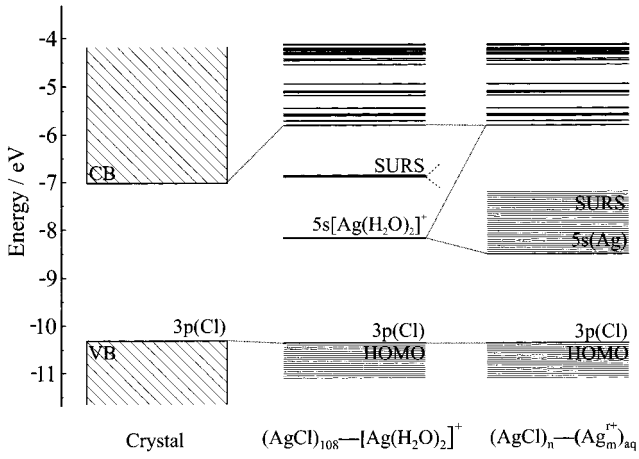

Figure 15. Comparison of the electronic structure of an infinite AgCl crystal, a nano cluster with one $[Ag(H_2O)_2]^+$ adsorbed on its surface, and one with several of them adsorbed, some of them already reduced and therefore represented as $(Ag_m{}^{r+})_{aq}$ with $r \leq m$. The crystal band gap and $(AgCl)_n-(Ag_m{}^{r+})_{aq}$ values correspond to experimental values.

The well-established difference of light sensitivity between single-crystal or very compact AgCl materials and of AgCl nanocrystals, on which Ag^+ ions have been adsorbed, have been investigated. Main features of the different electronic structures of an AgCl single crystal, a nano crystal with one $[Ag(H_2O)_2]^+$ adsorbed and a nano crystal on which several are adsorbed, some of them already reduced and therefore represented as $(Ag_m{}^{r+})_{aq}$ with $r \leq m$, are summarized in Figure 15. Properties of silver clusters and their role in silver halide photography have been investigated in detail by Henglein[50] and Belloni et al.[51] We have observed that placing an $Ag(H_2O)_2^+$ on all six faces of the $(AgCl)_{108}$, the oscillator strength of the first electronic transition, which is of 5s(Ag)←3p(Cl) CT type, rises more than six times with respect to $(AgCl)_{108}-[Ag(H_2O)_2]^+$ due to the cooperation between the adsorbed silver species. It is likely that these CT transitions are responsible for the well-established increased photochemical activity of nanocrystalline AgCl materials in the presence of an excess of silver ions.

Acknowledgment. We acknowledge financing support by the Schweizerisches Bundesamt für Energiewirtschaft BEW, project no. 10441, and by the Schweizerische Nationalfonds zur Förderung der wissenschaftlichen Forschung, project NF 2000-053414.98. We thank Dr. Ruedi Rytz, Dominik Brühwiler, Dr. Martin Brändle, and David Schürch for helpful discussions.

References and Notes

(1) Schaaf, L. J. *Out of the Shadows, Herschel, Talbot, & the invention of photography*; Yale University Press: New Haven, London, 1992.
(2) Ware, M. J. *IS&T's 48th Annu. Conf. Proc.* **1995**, 86.
(3) Pfanner, K.; Gfeller, N.; Calzaferri, G. *J. Photochem. Photobiol., A: Chem.* **1996**, *95*, 175.
(4) Saladin, F.; Kamber, I.; Pfanner, K.; Calzaferri, G. *J. Photochem. Photobiol., A: Chem.* **1997**, *109*, 47.
(5) Calzaferri, G. *Catalysis Today* **1997**, *39*, 145.
(6) Lanz, M.; Schürch, D.; Calzaferri, G. *J. Photochem. Photobiol., A: Chem.* **1999**, *120*, 105.
(7) Becquerel, E. *C. R. Acad. Sci.* **1839**, 561.
(8) James, T. H. *The Theory of the Photographic Process*, 4th ed.; Macmillan: New York, 1977.
(9) Aprà, E.; Stefanovich, E.; Dovesi, R.; Roetti, C. *Chem. Phys. Lett.* **1991**, *186*, 329.
(10) Scop, P. M. *Phys. Rev.* **1965**, *139*, A934.
(11) Bassani, F.; Knox, R. S.; Fowler, W. B. *Phys. Rev.* **1965**, *137*, A1217.
(12) Victora, R. H. *Phys. Rev. B* **1997**, *56*, 4417.
(13) Smith, P. V. *J. Phys. Chem. Solids* **1976**, *37*, 581.
(14) Hoffmann, R. *J. Chem. Phys.* **1963**, *39*, 1397.
(15) Calzaferri, G.; Forss, L.; Kamber, I. *J. Phys. Chem.* **1989**, *93*, 5366.
(16) Calzaferri, G.; Hoffmann, R. *J. Chem. Soc., Dalton Trans.* **1991**, 917.
(17) Calzaferri, G.; Rytz, R.; Brändle, M.; Brühwiler, D.; Glaus, S. *ICON-EDiT, Extended Hückel Molecular Orbital and Transition Dipole Moment Calculations*; available at http://iacrs1.unibe.ch (130.92.11.3), 1997, update 1998.
(18) Wolfsberg, M.; Helmholz, L. *J. Chem. Phys.* **1952**, *20*, 837.
(19) Brühwiler, D.; Gfeller, N.; Calzaferri, G. *J. Phys. Chem. B* **1998**, *102*, 2923.
(20) H_2O is an exception. It has been calculated with $\kappa = 1.0$ for the O−H and O−Ag^+(aq) interaction, and with $\kappa = 0.2$ for the H−H interaction.
(21) McGlynn, S.P.; Vanquickenborne, L. G.; Kinoshita M.; Carroll, D. G. *Introduction to Applied Quantum Chemistry*; Holt, Rinehart and Winston, Inc.: New York, 1972.
(22) Basch, H.; Viste A.; Gray, H. B. *Theor. Chim. Acta* **1965**, *3*, 458.
(23) Moore, C. E. *Atomic Energy Levels, Vol 3*; National Bureau of Standards: Washington, DC, 1971.
(24) Brändle, M.; Rytz, R.; Calzaferri, G. *BICON−CEDiT, Extended Hückel Tight-Binding and Crystal Transition Dipole Moment Calculations;* available at http://iacrs1.unibe.ch (130.92.11.3), 1997, update 1998.
(25) Brändle, M.; Calzaferri, G. *Helv. Chim. Acta* **1993**, *76*, 924.
(26) Calzaferri, G.; Rytz, R. *J. Phys. Chem.* **1995**, *99*, 12141.
(27) Hoffmann, R. *Solids and Surfaces: a chemist's view of bonding in extended structures*; VCH: New York, 1988.
(28) MacDonald, A. H. *Phys. Rev. B* **1978**, *18*, 5897.
(29) Mironov, V. E. *Radiokhimiya* **1962**, *4*, 707.
(30) Brühwiler, D.; Seifert, R.; Calzaferri, G. *J. Phys. Chem. B*, submitted for publication.
(31) Huber, K. P.; Herzberg, G. *Constants of Diatomic Molecules;* van Nostrand Reinhold Company: New York, 1979.
(32) Vonbacho, S.; Saltsburg, H.; Ceasar, G. P. *J. Electron Spectrosc. Relat. Phenom.* **1976**, *8*, 359.
(33) Rabin, I.; Jackschath, C.; Schulze, W. *Z. Phys. D: At., Mol. Clusters* **1991,** *19*, 401.
(34) Kirchhoff, F.; Holender, J. M.; Gillan, M. J. *Phys. Rev. B* **1994**, *49*, 17420.
(35) Huzinaga, S.; Klobukowski, M.; Barandiarán, Z.; Seijo, L. *J. Chem. Phys.* **1986**, *84*, 6315.
(36) Vogl, E.; Waidelich, W. *Z. Angew. Physik* **1968**, *25*, 98.
(37) Aline, P. G. *Phys. Rev.* **1957**, *105*, 406.
(38) Catalano, I. M.; Cingolani, A.; Lepore, M. *Phys. Rev. B* **1986**, *33*, 7270.
(39) Malik, A.-S.; DiSalvo, F. J.; Hoffmann, R.; Blair, J. T. *J. Imaging Sci. Technol.* **1998**, *42*, 210.
(40) Deng, H.; Kebarle, P. *J. Phys. Chem. A* **1998,** *102*, 571.
(41) Tsutsui, Y.; Sugimoto, K.; Wasada, H.; Inada, Y.; Funahashi, S. *J. Phys. Chem. A* **1997**, *101*, 2900.
(42) Martínez, J. M.; Pappalardo, R. R.; Sánchez Marcos, E. *J. Phys. Chem. A* **1997**, *101*, 4444.
(43) Holland, P. M.; Castleman, A. W., Jr. *J. Chem. Phys.* **1982**, *76*, 4195.
(44) Yamaguchi, T.; Johansson, G.; Holmberg, B.; Maeda, M.; Othaki, H. *Acta Chem. Scand. A* **1984**, *38*, 437.
(45) Texter, J.; Hastreiter, J. J.; Hall, J. L. *J. Phys. Chem.* **1983**, *87*, 4690.
(46) Seifert, R.; Kunzmann, A.; Calzaferri, G. *Angew. Chem.* **1998**, *110*, 1603.
(47) Purcell, K. F.; Kotz, J. C. *Inorganic Chemistry*; W. B. Saunders Company: Philadelphia, 1977.
(48) Tamm, I. *Z. Physik* **1932**, *76*, 849.
(49) Brändle, M.; Calzaferri, G.; Lanz, M. *Chem. Phys.* **1995**, *201*, 141.
(50) Henglein, A. *J. Phys. Chem.* **1993**, *97*, 5457.
(51) Belloni, J.; Mostafavi, M.; Marignier, J. L.; Amblard, J. *J. Imaging Sci.* **1991**, *35*, 68.